Waste and Biomass Valorization (2021) 12:1633–1646
https://doi.org/10.1007/s12649-020-01076-4

ORIGINAL PAPER

# Preparation of Paste Backfill Material from Mix-Calcined Sludge Ash

Qianming Lu[1] · Shuai Zhang[2] · Guangzhong Sun[1] · Xueqing Wang[1] · Shaojun Fu[1]

Received: 5 December 2019 / Accepted: 16 April 2020 / Published online: 15 May 2020


## Abstract

Paper mill sludge ash (PMSA) and sewage sludge ash (SSA) were mixed and calcined at high temperatures to improve the hydration activity of the sludge ash. The resulting mixture was utilized as an auxiliary cementing material to prepare backfill material for mining. Factors, including sludge ash mixing ratio and calcination temperature, affecting the properties and microstructure of the mixed calcinated sludge ash (MCSA) and cement paste were analyzed. Both raw materials and prepared cement pastes were characterized by different techniques, including XRD, FTIR, TG–DSC, SEM, and EDS. Results show that the major reaction products of PMSA and SSA mixture calcined at high temperature are gehlenite and belite, which exhibit high hydration activity in the pozzolanic reaction and significantly improve the degree of hydration of the MCSA–cement system. Compared with trials involving separate calcination of the two sludge ashes, pastes prepared by mixing calcination had a lower water demand, shorter setting time, and higher compressive strength. The amounts of $Ca(OH)_2$ and C–A(F)–S–H gel produced by the MCSA–cement hydration reaction increased, and the degree of polymerization of the gel phase improved with the increase in calcination temperature as well as the decrease in PMSA mixing ratio, which resulted in the formation of a dense microstructure at the later stage of hydration. This research also suggested that the best modulus range values of MCSA should be controlled to within $1.42 \leq HM \leq 1.48$ and $SM = 0.72$, the optimal calcination temperature was 1200 ℃, and the appropriate replacement rate of MCSA for cement should be equal to or smaller than 40% in laboratory conditions.

## Graphic Abstract

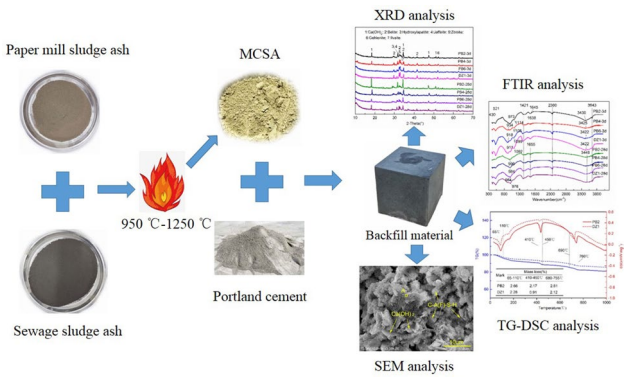


**Keywords** Paper mill sludge ash · Sewage sludge ash · Backfill material for mining · Hydration products · Mixed calcination

✉ Qianming Lu
luqianming134@126.com

[1] School of Safety Engineering, Henan University of Engineering, 1 Xiang He Road, Zhengzhou 451191, Henan, People's Republic of China

[2] School of Civil Engineering, Beijing Jiaotong University, 3 Shang Yuan Village, Beijing 100044, People's Republic of China

## Statement of Novelty

This work provided a new method for reuse of paper mill sludge ash and sewage sludge ash as a cement admixture with which to prepare paste backfill material. In general, the strength performance of hardened sludge ash-cement paste

will be significantly reduced by excessive addition of sludge ash. This work is innovative in that we mixed paper mill sludge ash and sewage sludge ash in certain proportions and calcined them at high temperature to form active minerals, which significantly improved the compressive strength of the sludge ash-cement paste. The preparation of this paste backfill material is conducive to realizing the large-scale reutilization of paper mill sludge and sewage sludge.

## Introduction

Paper mill sludge, one of the largest industrial solid wastes by mass, is produced during the process of pulping papermaking wastewater disposal whose annual discharge reaches over 12 million tons in China. Paper mill sludge contains a large amount of organic matters, heavy metals, and pathogens posing severe threats to the ecological environment and human health unless harmless disposal is effected [1–4]. The traditional methods of"dealing with paper mill sludge includes landfill, marine dumping, and incineration, among which, landfill occupies massive land resources and may cause groundwater pollution, marine dumping poses a serious threat to the marine ecological system and the human food chain, therefore, both methods are not considered to be environmentally friendly. By contrast, incineration treatment can significantly reduce sludge volume, kill pathogens, and improve heavy metal stability, thus comprising a comprehensive harmless handling method [5–9].

Paper mill sludge contains lots of $CaCO_3$, and small amounts of $SiO_2$ and $Al_2O_3$, the $CaCO_3$ will be decomposed into CaO with weak hydraulicity under high temperature, nevertheless, paper mill sludge ash (PMSA), if being used as a cement admixture, can substantially reduce the early strength of cement given excessive addition, furthermore, many pores in PMSA (formed by calcining) increase the water demand and lower the flow property of PMSA-cement paste [10], therefore, it is inapplicable to use PMSA alone as a cement admixture. The major components of sewage sludge ash (SSA) are $SiO_2$, $Al_2O_3$, CaO, and $Fe_2O_3$, among which, the non-crystal components have certain pozzolanic activity which can serve as supplementary cementing material to replace cement. Based on previous research into SSA, it is accepted that SSA has weak pozzolanic activity, a small amount substitution of SSA for cement rarely affects the compressive strength, while excessive SSA addition can markedly reduce the early strength of cement mortar. Martin et al. [11] suggested in their research that, the calcined sewage sludge possessed certain pozzolanic activity, and a small portion of SSA reacted with calcium hydroxide to produce calcium silicoaluminate. Jamshidi et al. [12] analyzed the SSA phase composition and pozzolanic activity, also exploring the influence of calcination on its crystallinity. Their research suggested that, the addition of SSA reduced the density and compressive performance of concrete, as well as improving the pore water adsorption. Cyr et al. [13] determined the properties of SSA-containing cement mortar and discovered that, compared with control mortars, SSA reduced the mortar compressive and flexural strengths, while such reductions were gradually weakened with time. Joo [14] reported that the strength of mortar with 10% addition of SSA was similar to, or higher than that of a pure cement test specimen. Chen et al. [15] obtained satisfactory compressive strength by substitution of 10% cement and 2% sand with SSA when preparing concrete mixes.

Cement clinker has excellent hydraulicity due to its high hydration activity components include tricalcium silicate ($C_3S$), bicalcium silicate ($C_2S$), tricalcium aluminate ($C_3A$), and tetracalcium aluminoferrite ($C_4AF$). Typically, these minerals are produced by the melting reaction of Ca provided by limestone, as well as Si and Al provided by clay at high temperature. Dry sewage sludge shares similar components with clay, and can replace part thereof to prepare Portland cement clinker with little influence on its performance. Lin et al. [16] used industrial sludge and waterworks sludge to replace some of raw materials used for preparing clinkers, and the results suggested that the calcination products had the same major mineral phases as silicate clinkers, including $C_3S$, $C_2S$, $C_3A$, and $C_4AF$, the results were consistent with those of Lin et al. [17]. Shih et al. [18] discovered that addition of sludge to less than 15% had little influence on clinker quality, and the $C_3S$ content in the clinker was apparently reduced as the dose was increased. Yang et al. [19] used 15–30% wastewater treatment plant sludge to replace some of the clay to prepare cement clinker. The result showed that the mineral structure, and hardening and hydration processes of prepared clinker were identical to those in Portland cement.

SSA, which serves as a cement admixture or replacement for clay when preparing cement clinker can effectively realize resourceful utilization of sewage sludge: however, the added amount of SSA should be controlled to within a small range due to its low pozzolanic activity, hindering the application of SSA. Paste backfill materials used for mining work may be classified as a type of mass concrete, which can be prepared to fill the goaf formed after coal mining for supporting the coal seam-roof, preventing surface subsidence, protecting buildings above mined areas, and protecting vegetation and groundwater aquifers from damage and even destruction [20–23]. The traditional filling paste materials used for mining works utilize cement, fly ash, and slag as cementing materials, the coal gangue and sand as aggregates, which are mixed with water and filled into the goaf. The price of backfill raw materials increases with the increasing amount of waste admixture such as fly ash and slag, thus hindering the popularization and application

of this backfill mining technology in Chinese coal mines [24–26]. The preparation of backfill material can realize the resourceful utilization of PMSA and SSA at a large-scale, reduce sludge-induced environmental pollution, decrease the costs of paste filling material, and hence reaping favorable environmental and economic benefits.

PMSA and SSA share similar compounds with limestone and clay, respectively, however, there has been no report on the products of PMSA and SSA and their reaction at high temperature and whether it will improve the hydration activity of the mixture, or not. This study attempted to mix PMSA and SSA for subsequent calcination at high temperature to improve the hydration activity of the sludge ash, and prepare a backfill paste material for mining engineering purposes. To this end, the work involved the investigation of the effects of SSA and PMSA mixing ratio and calcination temperature on the properties of MCSA–cement paste, such as compressive strength, setting time, and normal consistency water demand. In addition, X-ray diffraction (XRD), infrared spectroscopy, scanning electron microscopy (SEM), and thermogravimetric-differential scanning calorimetry (TG–DSC) were utilized to investigate the mineral composition, chemical structure, and microstructural evolution of MCSA–cement hydration products.

## Materials and Methods

### Materials

The paper mill sludge used in this study was sampled from the Dongxin Paper Mill in Henan Province, China. It was compressed into blocks using an extruding-desiccating machine in the paper mill with a water content of 53.5% and ignition loss of 35.7% at 600 °C. The sewage sludge was supplied by the Jinmen sewage treatment plant in Henan Province with a water content of 83.5% and ignition loss of 43.7% at 600 °C. To reduce the organic content of the sludge and promote tight contact between mixed sludge ash particles (thus facilitating the melting reaction), the raw sludges were dried to constant weight at 105 ℃, ground into powder (particle size < 0.8 μm), and calcined for 30 min at 600 ℃ in a muffle furnace. The resulting ashes were cooled at room temperature and ground again. The specific surface area of the resulting powder was 350–380 $m^2$/kg.

The chemical compositions of the PMSA and SSA were determined using X-ray fluorescence (XRF) spectroscopy, giving the results shown in Table 1. The oxides CaO, $Al_2O_3$, and $SiO_2$ were the most abundant ones found in the PMSA, while those in the SSA were $SiO_2$, $Al_2O_3$, CaO, $Fe_2O_3$, and $P_2O_5$. The XRD results obtained for the two raw materials (after calcination for 30 min at 600 °C) are shown in Fig. 1. Combining these results suggests that the Ca in the PMSA came mainly from $CaCO_3$ crystals that were preserved in the sludge during the papermaking process (calcite and aragonite powders were added during the papermaking process to improve the evenness and smoothness of the paper and further increase the paper's whiteness, opacity, printability, and size stability [27, 28]). Furthermore, the Si and Al in the PMSA were mainly distributed in the form of quartz ($SiO_2$) and corundum ($Al_2O_3$), respectively.

The major mineral components in the SSA were quartz, newberyite ($MgHPO_4(H_2O)_3$), CaO, and mitridatite ($Ca_6(H_2O)_6{\cdot}Fe_9O_6(PO_4)_9{\cdot}3H_2O$). The Fe that occurred in the mitridatite came from the ferric chloride used in the urban and domestic sludge treatment processes.

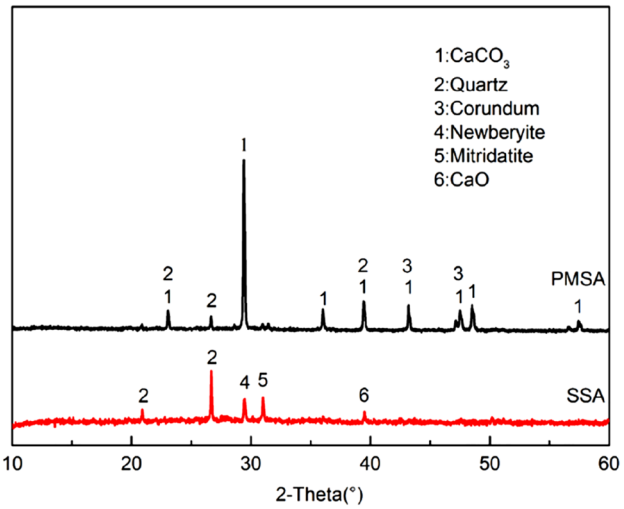


**Fig. 1** XRD pattern of raw paper mill sludge ash and sewage sludge ash

**Table 1** The chemical compositions of the PMSA and SSA (% by mass)

| Raw material/oxides | CaO | $Al_2O_3$ | $SiO_2$ | $Fe_2O_3$ | $SO_3$ | MgO | $P_2O_5$ | $Na_2O$ | $K_2O$ | LOI[a] |
|---|---|---|---|---|---|---|---|---|---|---|
| PMSA | 40.57 | 8.13 | 7.22 | 2.45 | 1.40 | 1.68 | 1.07 | 0.81 | 0.19 | 35.72 |
| SSA | 7.81 | 12.73 | 16.30 | 7.76 | 1.55 | 2.06 | 5.62 | 0.41 | 1.23 | 43.65 |

[a]Loss on ignition at 600 °C (%)

### Preparation of the MCSA

PMSA and SSA samples were evenly mixed together in a planetary mixer. On the basis of the results of preliminary experiments, the PMSA content was designed to be 77–87% of the total mass of the mixture with a interval of 2%; the corresponding mass percent of SSA was therefore 13–23%. The mixed sludge ash was then molded into cylinders measuring ∅ 3 cm × 1 cm using a pressure of 40 MPa, placed in a muffle furnace and calcined at 950–1250 °C with a interval of 50 °C for 30 min, cooled to room temperature, and ground into powder. The specific surface area of the MCSA powder thus acquired was 360–390 $m^2$/kg. The calcination quality of the MCSA was evaluated by using the XRF data to calculate its hydraulic modulus (HM) and silica modulus (SM) using the expressions:

$$HM = \frac{CaO}{SiO_2 + Al_2O_3 + Fe_2O_3} \quad (1)$$

$$SM = \frac{SiO_2}{Al_2O_3 + Fe_2O_3} \quad (2)$$

When investigating the effect of varying the mixing ratio, the calcination temperature were fixed at 1200 ℃. The corresponding MCSA samples were labeled RPB1–6 (amount of PMSA added from 77 to 87%, respectively). When exploring the effect of calcination temperature, the mixing ratio was fixed at that which produced the maximum compressive strength. The corresponding MCSA samples were labeled RTB1–7 (calcination temperature from 950 to 1250 ℃, respectively). Moreover, PMSA and SSA samples were separately calcined for 30 min at 1200 ℃ and mixed in a ratio of 79:21 (PMSA:SSA by weight) to prepare a control sample labeled RDZ1.

### Preparation of the MCSA–cement paste

MCSA–cement paste was prepared from a mixture of MCSA, reference cement, and water (at a fixed ratio of 2:3:2). The reference cement used was P·I 42.5 Portland cement consisting of 95% cement clinker and 5% gypsum which conforms to Chinese National Standard GB 175-2007 [29]. The MCSA and reference cement were first mixed together and then blended with water in a planetary mixer using a stirring rate of 120 r/min for 120 s.

Fresh paste was cast into cubic molds (40 × 40 × 40 $mm^3$) and vibrated for 5 min on a vibrostand to expel bubbles. The paste samples were then cured in a standard curing box at a constant temperature of 20 ℃ (and humidity of 95%) for 24 h. They were then removed from the molds and further cured for several (3 or 28) days. The cured blocks were then tested to determine their strengths.

Other fresh paste samples were cast into 20 × 20 × 20 $mm^3$ molds and used for microstructure analysis experiments. Paste samples PB1–6, TB1–7, and DZ1 were prepared using RPB1–6, RTB1–7, and RDZ1 samples, respectively, using the same method used for the MCSA–cement samples. In addition, control sample DZ2 was prepared using pure cement (like the other control sample).

### Paste Performance and Micro-testing

Three prime properties of the MCSA–cement paste (compressive strength, standard consistency water demand, and setting time) were examined based on the requirements stipulated for use in backfill mining. Compressive strength was determined using a hydraulic press (150 kN capacity and 0.6 MPa/s loading speed). Each strength value was determined three times and the results averaged. The standard consistency water demand and the setting times were determined using Vicat apparatus according to the method specified in Chinese National Standard GB/T 1346–2011 [30].

The chemical compositions of the PMSA and SSA calcined at 600 °C were determined using XRF spectroscopy. The mineral compositions of the MCSA and hardened MCSA–cement pastes were determined using an X-ray diffractometer (Rigaku Smartlab) and quantified using Rietveld refinement. Experiments were conducted using Cu Kα radiation at 40 kV and 30 mA at a scanning speed of 0.2°/min over a scanning range of 10° to 70°. Fourier-transform infrared (FTIR) spectra of the hardened MCSA–cement paste blocks were acquired using a Thermo Scientific Nicolet 6700 FTIR spectrometer (spectra were recorded at room temperature between 400 and 4000 $cm^{-1}$ with a resolution of 4 $cm^{-1}$). TG–DSC tests were carried out using a simultaneous thermal analyzer (Netzsch STA 449 F3) by heating the sample from 30 to 1000 °C at a rate of 10 °C/min under a nitrogen atmosphere. The micromorphology of the hydration products was investigated using a scanning electron microscope (SEM; Hitachi S-3400 N) employing an accelerating voltage of 15 kV and OCTANE PLUS energy spectrum analyzer (EDAX).

## Results and Discussions

### Effect of PMSA/SSA Mixed Ratio on Paste Samples

#### Performance of Pastes

Table 2 and Fig. 2 present the modulus values, compressive strengths, standard consistency water demand, and setting times of the MCSA–cement pastes (PB1–6) and control

**Table 2** Modulus values of the MCSA–cement pastes made using different mixing ratios

| Sample | PMSA:SA (by mass) | HM | SM |
|---|---|---|---|
| PB1 | 77:23 | 1.42 | 0.72 |
| PB2 | 79:21 | 1.48 | 0.72 |
| PB3 | 81:19 | 1.54 | 0.72 |
| PB4 | 83:17 | 1.60 | 0.71 |
| PB5 | 85:15 | 1.66 | 0.71 |
| PB6 | 87:13 | 1.73 | 0.71 |
| DZ1 | 79:21 | 1.47 | 0.72 |
| DZ2 | – | 2.03 | 2.10 |

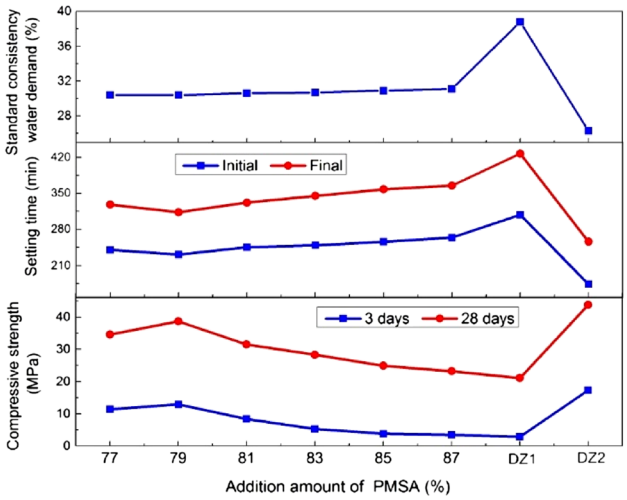


**Fig. 2** Effect of PMSA addition on the performance of MCSA–cement pastes

specimens (DZ1 and DZ2). The results indicate that sample DZ1 had the largest water demand (some 27.6% higher than that of sample PB2). It is also clear that the water demand of the MCSA–cement pastes increased slightly with increasing amount of PMSA. This may be attributed to the fact that the structure of the dry sludge is looser and more porous after calcination and its particles are increasingly more irregular. Thus, the specific surface area increases, as does its water-absorbing capacity. On the other hand, the high $P_2O_5$ content in SSA reduces the melting temperature of the minerals during calcination [31] and so a larger amount of liquid phase is produced which fills the micropores of the MCSA and results in a decrease in water demand.

The setting times of the MCSA–cement pastes were all less than that of DZ1. The shortest setting time was obtained when the PMSA:SSA ratio was 79:21 (i.e. group PB2). This result could be due to the greater early hydration activity of the MCSA which promotes the solidification process in the MCSA–cement paste systems. Furthermore, the PMSA in DZ1 has a stronger water-absorbing capacity, making it difficult for this system to obtain enough water to facilitate the hydration reaction. The setting times of the MCSA–cement pastes were also longer than that of the pure cement test sample (group DZ2), which is probably because the high cement content in DZ2 leads to the hydration reaction being particularly rapid.

It can also be seen from Fig. 2 that the compressive strength of the MCSA–cement paste increased at first and then decreased as the amount of PMSA increased. The maximum strength was found for group PB2 whose compressive strengths after 3 and 28 days were 344.8% and 83.4% higher than that of DZ1, respectively. Moreover, the compressive strengths of all of the MCSA–cement paste samples were superior to that of DZ1. These results suggest that the mixed calcination method substantially improves the hydration activity of the MCSA. This might be due to the formation of highly-activated minerals in the MCSA during the calcination process.

We also note that the compressive strengths of all the MCSA–cement pastes appear to be less than that of DZ2. For example, the compressive strengths of groups PB1 and PB2 were only 65.9% and 74.6% of that of DZ2 after 3 days, respectively, and the corresponding values for the other samples tested did not exceed 50%. This behavior could be due to slight hydration activity and high-water absorbing capacity of the MCSA particles. High levels of $P_2O_5$ in SSA will also promote the decomposition of $C_3S$ in the cement to $C_2S$, degrading the hydration performance of the cement and eventually weakening the compressive strength of the paste [32].

According to the analysis presented above, the best mixing ratio of the raw materials is 79:21 (PMSA:SSA by weight) and the corresponding modulus values should be HM = 1.42–1.48 and SM = 0.72.

## XRD Analysis

Figures 3 and 5 present the XRD diffractograms obtained from MCSA samples with different mixing ratios (i.e. RPB1–6 and control group RDZ1) and MCSA–cement hydration samples (PB1–6 and control group DZ1), respectively. Figure 4 present the Rietveld quantitative analysis of MCSA samples performed using GSAS EXPGUI. The profile were fitted using the Pseudo–Voigt function. The background was fitted graphically using the Shifted Chebyschev polynomial and the Rietveld results were normalized to 100% of the crystalline and amorphous phase, as can be seen, the Rwp in all the Rietveld refinements are smaller than 12%, indicating that the fitting results are reliable. It is clear from Fig. 3 that gehlenite ($2CaO{\cdot}Al_2O_3{\cdot}SiO_2$; $2\theta$ values of 24.26°, 26.11°, 31.68°, and 52.42°) and belite ($2CaO{\cdot}SiO_2$; $2\theta$ values of 29.67°, 33.17°, 37.89°,

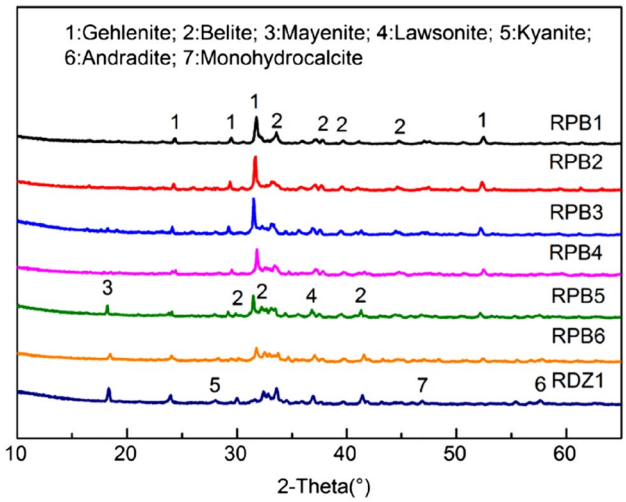


**Fig. 3** XRD pattern of MCSA with different mixing ratios

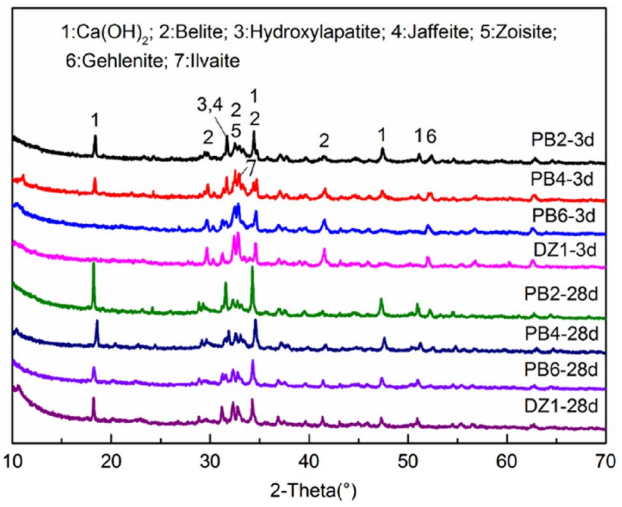


**Fig. 5** XRD pattern of MCSA–cement hydration samples made from different mixing ratios of MCSA

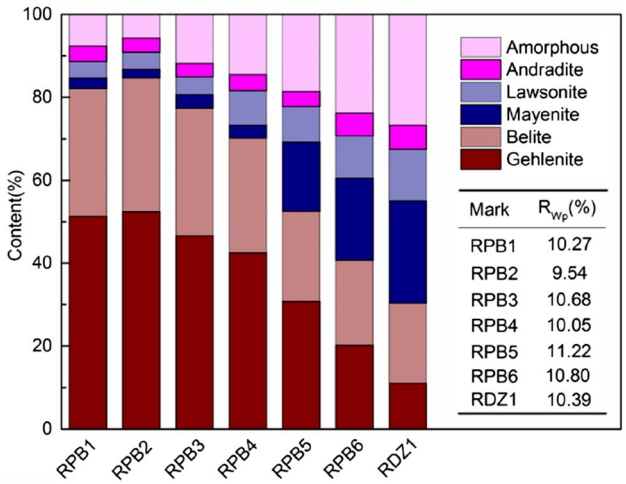


**Fig. 4** Mass fraction of mineral in MCSA samples with different mixing ratios

39.60°, 41.46°, and 44.67°) are the major phases present in the MCSA. In addition, some weak diffraction peaks due to mayenite ($12CaO{\cdot}7Al_2O_3$; $2\theta = 18.37°$), lawsonite ($CaAl_2Si_2O_7{\cdot}(OH)_2{\cdot}H_2O$; $2\theta = 36.92°$), kyanite ($Al_2SiO_5$; $2\theta = 28.10°$), andradite ($Ca_3Fe_2(SiO_4)_3$; $2\theta = 57.66°$), and monohydrocalcite ($CaCO_3{\cdot}H_2O$, $2\theta = 46.90°$) were also detected in the MCSA.

The intensities of the characteristic peaks due to gehlenite ($2\theta = 26.11°$, 31.68°, and 52.42°) and belite ($2\theta = 33.17°$) appeared to decrease as the added PMSA ratio increased (i.e. from RPB1 to RPB6), indicating a reduction in the amount of these crystal phases produced. For example, the content of gehlenite and belite in sample RPB6 are 61.5% and 36.5% less than that in sample RPB2, respectively. In contrast, only one weak gehlenite diffraction peak (with a content of 11%) could be detected (at $2\theta = 24.26°$) in the group RDZ1. This clearly indicates that the calcination of PMSA and SSA mixtures with appropriate ratios leads to an increase in the formation of gehlenite.

The XRD patterns of the hydrated MCSA–cement pastes presented in Fig. 5 show that the main phases present in the hydrated products are portlandite ($Ca(OH)_2$; $2\theta$ values of 18.32°, 34.34°, 47.36°, and 51.0°), zoisite ($Ca_2Al_3Si_3O_{12}(OH)$; $2\theta = 32.55°$), jaffeite ($Ca_6(Si_2O_7)(OH)_6$; $2\theta = 31.73°$), hydroxylapatite ($Ca_5(PO_4)_3(OH)$; $2\theta = 31.73°$), and ilvaite ($CaFe_3Si_2O_8(OH)$; $2\theta = 32.96°$). Portlandite and jaffeite are the typical hydration products formed when Portland cement is used. The formation of hydroxylapatite and ilvaite is probably due to the substitution of P and Fe (derived from SSA) in place of Si in jaffeite, which confirms that the SSA is involved in the hydration reaction. Moreover, weak peaks were also observed that can be ascribed to unreacted belite ($2\theta = 29.67°$, 33.17°, and 41.46°) and gehlenite ($2\theta = 52.42°$) that are presumably derived from sludge ash and unreacted cement particles. In this case, protuberant diffraction peaks indicating the presence of species of lower crystallinity occur in the region $2\theta = 27°$ to 35°. These suggest the presence of calcium silicate hydrate (C–S–H), calcium aluminosilicate hydrate (C–A–S–H), and calcium ferrite–silicate hydrate (C–F–S–H) gel phases in the hydration products [33–35].

The intensities of the portlandite peaks increase with the curing time and amount of SSA added (i.e. from PB6 to PB1), whereas the peaks due to belite and gehlenite present a decreasing trend, demonstrating the improvement obtained in the degree of hydration of the MCSA–cement system. The characteristic peaks due to portlandite in PB2 are sharper than those in DZ1, especially in the data recorded after

3 days of curing. Indeed, only a weak peak was observed in the DZ1 spectrum at $2\theta = 34.34°$, indicating that the PB2 samples had higher degrees of hydration than those in the DZ1 group. This also helps account for the higher compressive strength of the group PB2 samples after 3 days of curing.

According to Fig. 3, the major crystalline phases in the MCSA are gehlenite and belite. Belite possesses strong hydration activity and can directly react with water to produce $Ca(OH)_2$ and C–S–H gel [36, 37], which has a positive effect on the strength of the paste. Previous research has shown that gehlenite does not react chemically with water – however, it can (especially in the glassy phase) react with $Ca(OH)_2$ to produce C–A–S–H gels that have tough structures [38]. Therefore, the hardening process of the MCSA–cement system can be summarized as follows. First, the CaO, $SiO_2$, and $Al_2O_3$ in the MCSA interact with each other at high temperature to produce pozzolanic active minerals—belite and gehlenite. Then, C–A–S–H gels are produced due to the reaction between the gehlenite and $Ca(OH)_2$ provided by the hydration of $C_3S$ and $C_2S$ in the cement. This reaction eventually promotes the hydration reaction of $C_3S$ and $C_2S$, accelerating the hydration process of the MCSA–cement system and increasing the compressive strength of the system.

### FTIR Analysis

To supplement the XRD analysis, infrared spectroscopy can be used to investigate the amorphous phases involved in the hydration process. FTIR spectra of the hydrated MCSA–cement pastes are presented in Fig. 6.

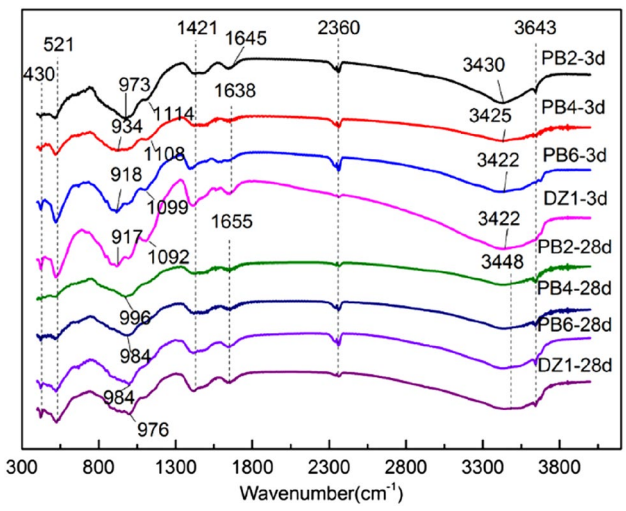


**Fig. 6** FTIR spectrum of MCSA–cement hydration samples made from different mixing ratios of MCSA

The absorption peaks at 430/521 and 925–934 $cm^{-1}$ correspond to the Si–O bending vibrations in $C_2S$ and asymmetric stretching vibrations in $C_3S$, respectively, indicating the presence of unreacted clinker particles in the test samples. The peaks at 973–996 $cm^{-1}$ are attributed to the Si–O stretching vibrations of the Q2 tetrahedra in C–S–H gel. Those at 1092–1114 $cm^{-1}$ are caused by amorphous aluminosilicate vibrations which confirms the presence of C–A–S–H gel (in agreement with the result of the XRD analysis). The carbonate bands at 1421 and 2360 $cm^{-1}$ are mainly due to atmospheric $CO_2$ reacting with the $Ca(OH)_2$ produced by the hydration of cement. The broad bands appearing at 3422–3448 $cm^{-1}$ and 1638–1655 $cm^{-1}$ are due to the bending vibrations of irregularly bound water [39–41]. The set of higher frequency peaks at 3643 $cm^{-1}$ are attributed to the O–H stretching vibrations in $Ca(OH)_2$ which is produced by the hydration of calcium silicate in the paste samples.

The FTIR results further show that the following changes can be discerned as the SSA mixing ratio and curing time increase: (i) The intensities of the $C_3S$ and $C_2S$ absorption peaks at 430 and 521 $cm^{-1}$ decrease significantly due to the hydration reaction of the calcium silicate in the MCSA–cement system. (ii) The 925 $cm^{-1}$ peak in the 3-day data shifts to a higher frequency (973 $cm^{-1}$) as does that at 976 $cm^{-1}$ in the 28-day data (which shifts to 996 $cm^{-1}$). This is caused by the dissolution of the calcium silicate to form C–S–H gel phases as hydration proceeds and simultaneously indicates the increasing degree of polymerization of the C–S–H gel [42]. (iii) The main bands due to bound water that appear at 1638 and 3422 $cm^{-1}$ shift to higher frequencies (1655 and 3448 $cm^{-1}$, respectively), indicating an increase in hydrated products associated with water. (iv) There is an increase in the intensity of the absorption peak at 3643 $cm^{-1}$ that is attributed to $Ca(OH)_2$ [43]. This indicates that there is an increase in the amount of $Ca(OH)_2$ produced which is in good agreement with the results of the XRD analysis.

## Effect of Calcination Temperature and MCSA Addition Ratio on Paste Samples

### Paste Performance

Figures 7 and 8 present graphs showing the change in performance of the MCSA–cement pastes (standard consistency water demand, setting time, and compressive strength) as the calcination temperature and amount of MCSA added are increased, respectively. As can clearly be seen, the standard consistency water demand of the MCSA–cement system gradually decreases as the calcination temperature is increased from 950 to 1250 °C. However, it remains inferior to that of the pure cement specimens. This may be due to the fact that the organic

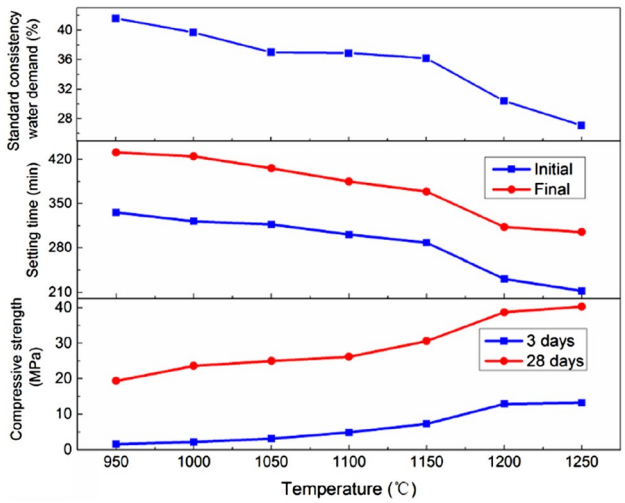


**Fig. 7** Effect of calcination temperature of MCSA on the performance of MCSA–cement pastes

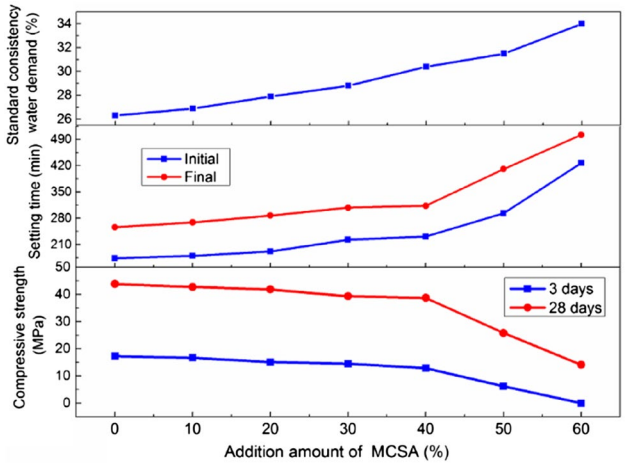


**Fig. 8** Effect of MCSA addition on the performance of MCSA–cement pastes

components and water in the sludge become volatilized at the high temperature during calcination, thus producing a large number of capillary pores. Such micropores could serve as water containers which, in turn, will lead to an increased water demand by the MCSA–cement system. Nevertheless, as the calcination temperature increases, more and more minerals in the sludge ash become involved in the melting reaction and the micropores in the MCSA will be filled with these molten minerals. Thus, the water demand of the MCSA–cement system decreases. This rationale also explains why the water demand decreases when the MCSA mixing ratio is increased. As the calcination temperature increases from 1150 to 1200 °C, the reactions occurring in the melting MCSA will become more vigorous which helps improve the micropore structure. Thus, there is a 16.0% reduction in the water demand in group RTB6 compared to group RTB5. The setting times of the MCSA–cement pastes clearly decrease as the calcination temperature increases. This is because higher calcination temperatures promote the formation of active minerals in the MCSA that accelerate the rates of the subsequent hydration reactions and thus shorten the setting time of the paste. The setting time becomes more prolonged, however, when the amount of MCSA is increased. This is probably due simply to the fact that the concentration of the cement decreases as the percentage of MCSA increases.

It can also be seen from Figs. 7 and 8 that there is an increase in compressive strength as the calcination temperature increases and MCSA percentage decreases. The compressive strengths of the MCSA–cement samples were quite unsatisfactory when calcination temperatures between 950 and 1150 °C were used, especially when they were cured for just 3 days. For example, the compressive strengths of samples formed using MCSA calcined at 950, 1000, 1050, 1100, and 1150 °C were only 9.25%, 12.72%, 17.92%, 28.32% and 42.2%of those of the pure cement specimen, respectively. Increasing the calcination temperature from 1150 to 1200 °C, however, produced a marked increase (76.47%) in the compressive strength of the specimens hardened for 3 days. This suggests that a significant improvement in the degree of hydration of the MCSA–cement system had been achieved by this change in calcination temperature, which might be due to a substantial increase in pozzolanic activity in the MCSA. We note, however, that a further increase in calcination temperature to 1250 °C yielded only a slight increase in the compressive strength of the hardened samples.

Figure 8 reveals that an MCSA substitution rate of 10% reduces the compressive strengths of samples aged for 3 and 28 days by 3.47% and 2.51% compared to pure cement specimens, respectively. The corresponding losses of strength when the MCSA ratio is increased from 40 to 50% are 51.94% and 33.33%, respectively, which are clearly significantly higher than those occurring between other groups. Moreover, at a substitution level of 60%, the specimens produced after aging for 3 days were too soft to be tested and hardly satisfied the strength requirements needed for use as backfill material in mining applications.

Overall, our results suggest that the amount of MCSA employed should be ≤ 40%. Moreover, the optimal calcination temperature is 1200 °C under laboratory conditions (higher temperatures consume more energy but do not significantly improve the performance of the MCSA–cement paste).

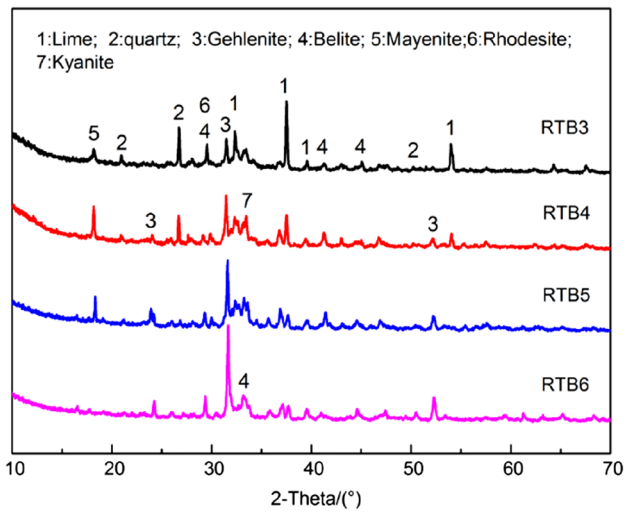


**Fig. 9** XRD pattern of MCSA calcined at different temperatures

## XRD Analysis

The results of the XRD analyses performed on MCSA samples produced at different calcination temperatures are shown in Fig. 9 and those on the hydrated samples of the various MCSA–cement systems are presented in Fig. 11. The Rietveld quantitative analysis of MCSA samples are shown in Fig. 10.

Figure 9 contains obvious characteristic peaks due to the presence of lime (CaO; $2\theta = 37.50°$, 32.34°, 39.53°, and 54.01°) when the calcination temperature is 1050 °C. This is due to the decomposition of $CaCO_3$ in the PMSA. Moreover, characteristic peaks due to unreacted quartz ($SiO_2$; $2\theta = 20.95°$, 26.73°, and 50.19°) and gehlenite ($2\theta = 31.68°$) can also be observed, suggesting a fraction of the SSA had been involved in the melting reaction at 1050 °C. The characteristic peaks due to lime and unreacted quartz gradually weaken as the calcination temperature increases. For example, the content of lime and quartz in sample RTB6 are 89.9% and 91.6% less than that in sample RTB3 respectively. However, the intensities of the gehlenite peaks are simultaneously enhanced, its content increased by 569.2% in RTB6 as compare with that in RTB3, indicating that the gehlenite is produced by the reactions occurring between the lime (Ca provider), quartz (Si provider), and mayenite (Ca and Al provider) as the temperature increases. Peaks due to belite ($2\theta = 29.54°$ and 41.26°) can also be observed at a calcination temperature of 1050 °C. The intensities of these peaks increase slightly as the calcination temperature is increased to 1200 °C, indicating that there is increased production of belite as the calcination temperature increases. This also helps improve the strength of the MCSA–cement system.

In the diffractograms of the hydrated MCSA–cement systems (Fig. 11), the most intense peaks are ascribed to portlandite and these are most pronounced at 1050 °C (see, for example, group TB3-28d). The formation of portlandite can be attributed to the hydration of the cement and free CaO in the MCSA. The intensities of the belite and gehlenite peaks decrease gradually as the calcination temperature and hydration time are increased, while the portlandite peaks are markedly enhanced at the same time (from 1150 to 1200 °C). This is indicative of the improvement in the degree of hydration of the MCSA–cement system due to the pozzolanic reaction of the gehlenite and hydration of the belite.

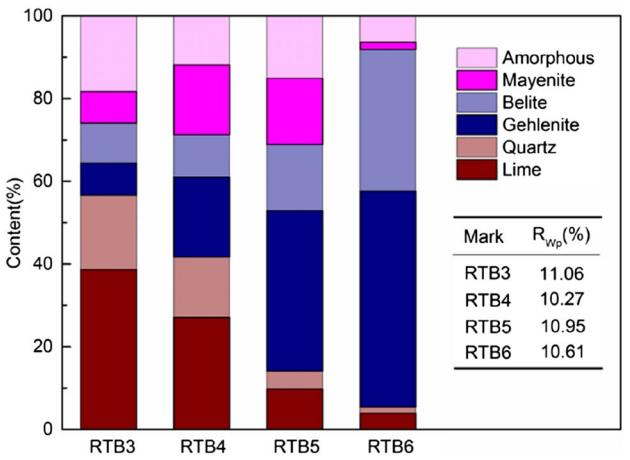


**Fig. 10** Mass fraction of mineral in MCSA samples calcined at different temperatures

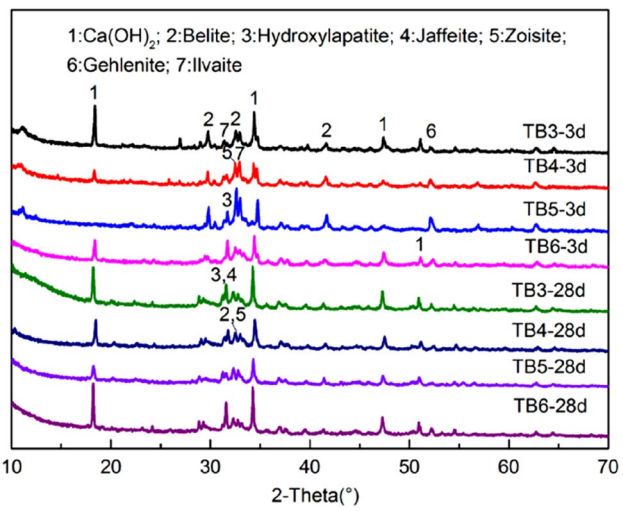


**Fig. 11** XRD pattern of MCSA–cement hydration samples made from MCSA calcined at different temperatures

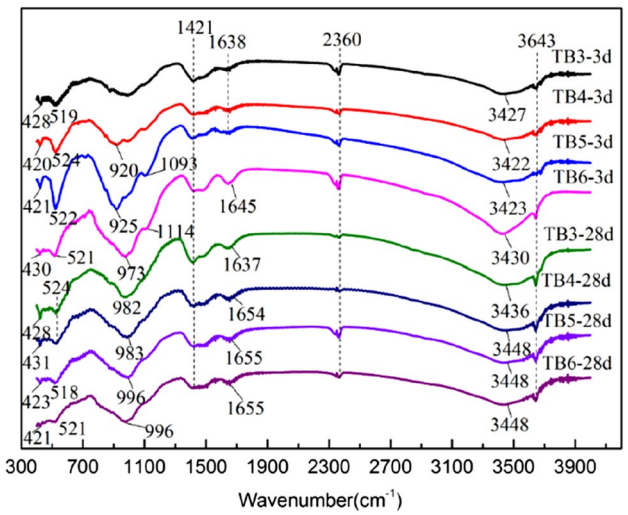


**Fig. 12** FTIR spectrum of MCSA–cement hydration samples made from MCSA calcined at different temperatures

### FTIR Analysis

The relevant FTIR spectra of the MCSA–cement pastes are given in Fig. 12. As the calcination temperature is increased from 1050 to 1200 °C, the following results can be observed: (i) the Si–O bending vibrations associated with $C_2S$ that occur between 420–431 and 518–524 $cm^{-1}$ become weaker, while those associated with irregularly bound water (observed at 1637–1655 $cm^{-1}$ and 3422–3448 $cm^{-1}$) gradually increase in intensity. Moreover, the peaks shift to higher frequencies, especially in the 3-day data and with temperatures from 1150 to 1200 °C. This indicates that more and more of the silicate phases in the MCSA and cement dissolve to form $Ca(OH)_2$, C–S–H, and C–S–A–H gels, which can be attributed to the formation of excess gehlenite and belite in the MCSA at higher temperatures. (ii) the main $C_3S$ and $C_2S$ bands that appear at 920 and 925 $cm^{-1}$ shift to higher frequencies in the region 973–996 $cm^{-1}$. This suggests there is an increase in the degree of C–S–H polymerization and better hydration of the SSA. In addition, the amorphous aluminosilicate vibration band that occurs at 1093 $cm^{-1}$ shifts to 1114 $cm^{-1}$ [44], indicating the presence of C–A–S–H gel and an increase in its degree of polymerization. This is also beneficial for the development of the strength of the paste. The C–A–S–H gel is mainly produced by the pozzolanic reaction between gehlenite and $Ca(OH)_2$. More gehlenite is formed as the calcination temperature of the MCSA increases, thus providing enough raw material for the pozzolanic reaction to occur.

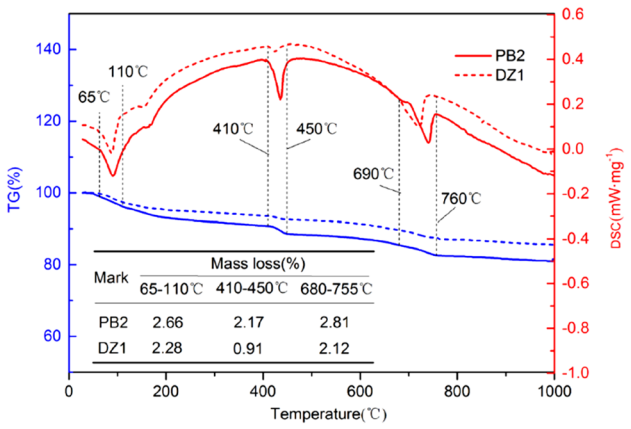


**Fig. 13** TG–DSC curve of hydration sample DZ1 and PB2 at 3 days

## TG–DSC Analysis

TG–DSC was utilized to quantitatively analyze the compositions of the MCSA–cement pastes (PB2/TB6) and control sample (DZ1) to further our study of the effect of MCSA calcination on the hydration process. The results are presented in Figs. 13 and 14.

As can be seen, the DSC curves of the samples exhibit three major endothermic peaks corresponding to three major weight loss stages in the TG curves. According to previous research [45–48], the loss of mass between 65 and 110 °C corresponds to the decomposition of ettringite. However, no ettringite could be detected by XRD in our experiments and so the mass loss in this region is more likely to be due to the loss of evaporable water and presence of poorly formed C–S–H gel. The mass lost between 410 and 450 ℃ corresponds to the decomposition of $Ca(OH)_2$, the presence of which is verified by the observation of $Ca(OH)_2$ peaks in the XRD and FTIR results. The mass losses observed are

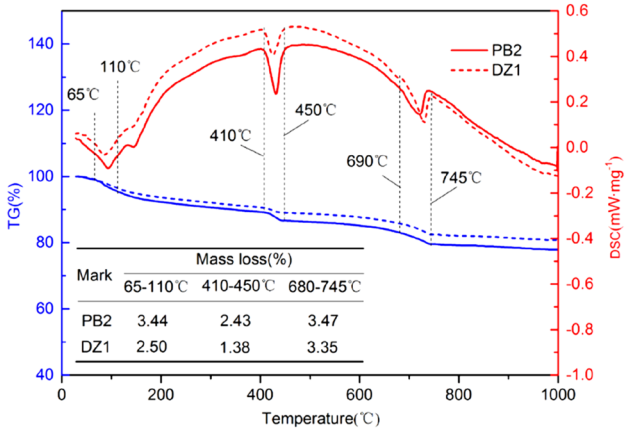


**Fig. 14** TG–DSC curve of hydration sample DZ1 and PB2 at 28 days

estimated to be 2.17% in PB2 and 0.91% in DZ1 (after curing samples for 3 days). This result is a strong indication of the apparent effect of the MCSA in promoting the hydration of the paste system. The result also shows that $Ca(OH)_2$ is present in group DZ1 which was not expected as it was not detected using XRD. This suggests that the $Ca(OH)_2$ is probably present in an amorphous form. Figure 14 shows that the mass lost by the PB2 group due to $Ca(OH)_2$ decomposition increases to 2.43% after 28 days. It is noted, therefore, that the production of $Ca(OH)_2$ in group PB2 is not reduced by the pozzolanic reactions occurring during 28 days of hydration. Thus, more $Ca(OH)_2$ must be produced by the hydration of the MCSA–cement system than is consumed in pozzolanic reactions.

The mass losses in the ranges 680–745 °C and 680–755 °C are associated with the decomposition of C–S–H, C–A(F)–S–H gel, and $CaCO_3$, which is generated from the reaction of $Ca(OH)_2$ with atmospheric $CO_2$. However, no characteristic peaks due to $CaCO_3$ are observed in the XRD spectra (see Fig. 5). Consequently, the mass losses in this temperature range can be mainly attributed to the decomposition of the gel phase produced by the hydration of the calcium silicate in the cement and the pozzolanic reaction of the gehlenite in the MCSA. In the 3-day data, the mass loss in this range from group PB2 was 32.55% larger than that from group DZ1, thus indicating that group PB2 contained more gel phase. This helps explain the marked increase in compressive strength observed in Fig. 2. After 28 days of hydration, however, the mass loss in PB2 due to the presence of the gel phase was only slightly larger than that lost by group DZ1 (a mere 3.58%). This explains why there was much less difference in the final compressive strengths of the PB2 and DZ1 samples.

The above results suggest that sludge ash prepared by a method involving mixing before calcination has a higher pozzolanic activity than that prepared by carrying out the calcination before mixing. The former case promotes the early hydration of the cement, while the promotion effect is weaker at the later hydration stage.

### SEM Analysis

Figure 15 shows SEM images of samples of DZ1 (Fig. 15a and b) and PB2 (Fig. 15c and d) recorded after 3 and 28 days. A large number of small, isolated particles can be seen in the hardening paste imaged in Fig. 15a. These are most likely to be unhydrated sludge ash or cement clinker particles in light of the XRD and FTIR results. The particles are not mutually fused together due to their low degree of hydration and form a loose structure with an abundance of pores.

In contrast, a large amount of 'cloud-like' hydration products can be observed in specimen PB2 (Fig. 15c) that have blurry edges and are covered by fine, irregular, burr-like crystals. The EDS data recorded from microregion A (Fig. 15e) indicate the presence of Ca, Si, O, Al, and Fe. Furthermore, the abundances of the elements are such that the Ca:Si:Al:Fe ratios are equal to 1:0.41:0.31:0.13 (by weight). Combining this information with the XRD results (see Fig. 5) reveals that the main phase of the hydration process involves the formation of C–A(Fe)–S–H gel in the hydrated sample. As the C–A(Fe)–S–H gel is produced by the pozzolanic reaction of the MCSA, this suggests that the pozzolanic reaction of the MCSA participates in the reaction at an early stage. The gel phase seems to evolve with increasing hydration time and tends to become more integrated. In addition, flakes of $Ca(OH)_2$ crystals can be observed in Fig. 15c that are 5–10 μm in diameter and approximately 1 μm thick. These appear to be tightly wrapped within the C–A(Fe)–S–H gel, leading to a dense structure.

After being cured for 28 days, the gel phase produced in sample DZ1 appears to have kept on growing (Fig. 15c), the particles becoming more integrated with each other as well as leaving many pores. The EDS results from point B (Fig. 15f) indicate that the elements Al and Fe present in the gel phase (which mainly derive from the sludge ash) only account for 1.56% and 0.53% of the sample by weight, respectively. These proportions are much less than those found in group PB2 and indicate that only a tiny amount of sludge ash participates in the pozzolanic reaction in DZ1. The hydration product in group DZ1 is therefore dominated by C–S–H gel and is mostly produced by the hydration of the $C_3S$ and $C_2S$ in the cement. Flakey crystals of $Ca(OH)_2$ can also be observed in this gel but they have a thickness of less than 0.5 μm and a lower degree of development.

Figure 15d shows that the major phase present in sample PB2 at this late stage of development is C–A(Fe)–S–H gel produced by the pozzolanic reaction of MCSA. The pores of the sample are filled, hardening the sample and leading to a more compact microstructure. This accounts for the high compressive strength of the group PB2 samples compared to those in group DZ1.

## Conclusions

In this study, PMSA and SSA were mixed together and calcined to obtain a product with higher hydration activity. The effect of varying the mixing ratio and calcination temperature of the raw sludge ash on the mineral composition of the MCSA was investigated. The changes in the physicochemical properties and microstructures of the MCSA–cement systems were also examined. The following conclusions may be drawn on the basis of the results obtained:

1. As the amount of SSA added is increased, more gehlenite and belite are produced in the melting reaction

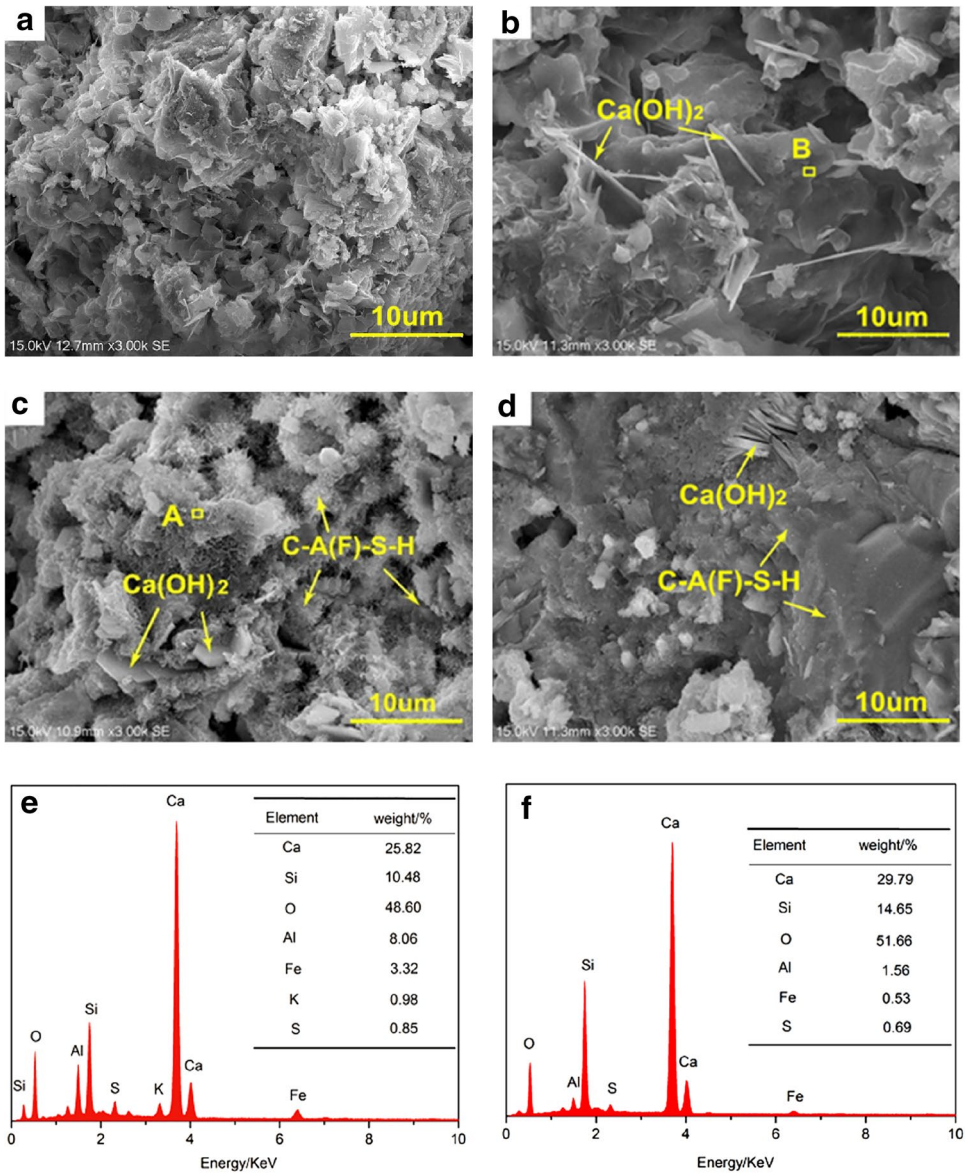


**Fig. 15** SEM micrographs and EDS analysis of hydration samples: **a** sample DZ1 at 3 days, **b** sample DZ1 at 28 days, **c** sample PB2 at 3 days, **d** sample PB2 at 28 days, **e** EDS analysis of micro-region A, **f** EDS analysis of micro-region B

between the PMSA and SSA. This further promotes the generation of $Ca(OH)_2$, C–S–H, and C–A(Fe)–S–H gel during the hydration of the MCSA–cement system; it also increases the degree of polymerization of the gel phase. Among all of the MCSA mixing ratio schemes used, sample PB2 has the smallest water demand, shortest setting time, and the highest compressive strength. More specifically, cured samples were found to be 344.8% (after 3 days) and 83.4% (after 28 days) stronger than the corresponding control samples. The optimal values of the moduli of the MCSA are suggested to be HM = 1.42–1.48 and SM = 0.72 under laboratory conditions.

2. As the calcination temperature of the MCSA is increased, the water demand of the MCSA–cement paste decreases, the setting time becomes shorter, and the compressive strength is substantially enhanced. The XRD and FTIR results suggest that gehlenite and belite are produced by reactions that occur between minerals such as lime, quartz, and mayenite in the MCSA at high temperature. More gehlenite and belite are produced as the calcination temperature increases, especially from 1150 to 1200 °C, which also promotes the hydration reaction of the MCSA–cement system. Overall, considering the need to save energy, 1200 °C is suggested as the optimal calcination temperature for the MCSA. Moreover, the addition of an excessive amount of MCSA can substantially reduce the strength of the cured cement paste: the amount added should, therefore, be ≤ 40%.
3. TG–DSC and SEM–EDS results suggest that MCSA–cement pastes prepared from calcined samples of mixed PMSA and SSA produce more $Ca(OH)_2$ and C–A(Fe)–

S–H gel compared with samples separately calcined. Both of these products are derived from the pozzolanic reaction of the gehlenite in the MCSA. The gel phase evolves and mutually fuses together to form a dense structure as the hydration time is prolonged and this enhances the strength of the MCSA–cement paste.

**Acknowledgements** This study was supported by the Science and Technology Research Project of Henan province (Grant No. 19210231046), Key Scientific Research Funding Project for Colleges of Henan Province (Grant No. 18A440007), and Doctoral Foundation Project of Henan University of Engineering (Grant No. D2017003). The authors also would like to thank the editors and reviewers for their detailed comments and helpful suggestions.

## References

1. Jiang, J., Ma, X.: Experimental research of microwave pyrolysis about paper mill sludge. Appl. Therm. Eng. **31**, 3897–3903 (2011)
2. Cheng, S., Liu, Y., Chen, Q., Deng, X., Peng, P.Q., Liao, B.H.: Effect of applied paper mill sludge on migration of Cd in soil-white radish system. Chin. J. Environ. Eng. **11**(3), 1907–1910 (2017)
3. Han, Q., Ruan, X.J., Zhang, T.: Study on technology of paper sludge backfilling into paper web. J. Shanxi Univ. Sci. Technol. (Nat. Sci. Ed.) **34**(6), 25–28 (2016)
4. Hu, Z.S., Deng, Y.L.: Supersaturation control in aragonite synthesis using sparingly soluble calcium sulfate as reactants. Colloid Interface Sci. **266**(2), 359–365 (2003)
5. Vegas, I., Frías, M., Urreta, J.: Obtaining a pozzolanic addition from the controlled calcination of paper mill sludge: performance in cement matrices. Mater. Constr. **56**(283), 49–60 (2006)
6. Jesús, A.G., Ochoa, D.A.: Feasibility of recycling pulp and paper mill sludge in the paper and board industries. Resour. Conserv. Recycl. **52**(7), 965–972 (2008)
7. Zhang, L.H., Xu, C.B., Champagne, P.: Energy recovery from secondary pulp/paper-mill sludge and sewage sludge with supercritical water treatment. Bioresour. Technol. **101**(8), 2713–2721 (2010)
8. Liao, Y.F., Ma, X.Q.: Thermogravimetric analysis of the co-combustion of coal and paper mill sludge. Appl. Energy **87**(11), 3526–3532 (2010)
9. Cavdar, A.D., Yel, H., Boran, S., Pesman, E.: Cement type composite panels manufactured using paper mill sludge as filler. Constr. Build. Mater. **142**(1), 410–416 (2017)
10. Lu, Q.M., Zhang, Y.X., Sun, W.B., Han, H.Q., Wang, Z.C.: A proportioning testing method for preparing the coal mine filling cementi-tious materials with the paper mill sludge ash. J. Saf. Environ. **18**(6), 2357–2362 (2018)
11. Martin, C., Coutan, D.M., Clastres, P.: Technological and environmental behavior of sewage sludge ash (SSA) in cement-based materials. Cem. Concr. Res. **37**(8), 1278–1289 (2007)
12. Jamshidi, M., Jamshidi, A., Mehrdadi, N.: Mechanical performance and capillary water absorption of sewage sludge ash concrete (SSAC). Int. J. Sustain. Eng. **5**(3), 227–228 (2012)
13. Cyr, M., Coutand, M., Clastres, P.: Technological and environmental behavior of sewage sludge ash (SSA) in cement-based materials. Cem. Concr. Res. **37**(8), 1278–1289 (2007)
14. Joo, H.T.: Sludge ash as filler for portland cement concrete. J. Environ. Eng. **113**(2), 345–349 (1987)
15. Chen, M., Blanc, D., Gautier, M., Mehu, J., Gourdon, R.: Environmental and technical assessments of the potential utilization of sewage sludge ashes (SSAs) as secondary raw materials in construction. Waste Manage. **33**(5), 1268–1275 (2013)
16. Lin, K.L., Lin, C.Y.: Hydration characteristics of waste sludge ash utilized as raw cement material. Cem. Concr. Res. **35**(10), 1999–2007 (2005)
17. Lin, Y.M., Zhou, S.Q., Zhou, D.J., Wu, Y.Y.: Utilizing the wastewater treatment plant sludge for the production of eco-cement. Environ Sci. **32**(2), 524–528 (2011)
18. Shih, P.H., Chang, J.E., Lu, H.C., Chianga, L.C.: Reuse of heavy metal-containing sludges in cement production. Cem. Concr. Res. **35**(11), 2110–2115 (2005)
19. Yang, L.Y., Yang, J., Ma, J.T.: Research on the preparation of cement clinker utilizing the sludge of sewage treatment plants. J. Wuhan Univ. Technol. **29**(11), 11–13 (2007)
20. Yao, Y., Sun, H.H.: A novel silica alumina-based backfill material composed of coal refuse and fly ash. J. Hazard. Mater. **213**, 71–82 (2012)
21. Huang, Y.L., Zhang, X.J., Zhang, Q., Nie, S.J.: Backfilling technology of substituting waste and fly ash for coal underground in china coal mining area. Environ. Eng. Manage. J. **10**(6), 769–775 (2011)
22. Yao, Y., Sun, H.H.: Characterization of a new silica alumina-based backfill material utilizing large quantities of coal combustion byproducts. Fuel **97**, 329–336 (2012)
23. Miu, X.X., Ju, F., Huang, Y.L.: New development and prospect of backfilling mining theory and technology. J. China Univ. Min. Technol. **44**(3), 391–399 (2015)
24. Deng, D.Q., Yao, Z.H., Zhu, Y.J., Wang, L.H.: Forecasting cemented backfill strength: Back calculation of cement dosage. J. China Univ Min. Technol. **42**(1), 39–44 (2013)
25. Zhang, Q.L., Li, X.P., Yang, W.: Preparation and hydrated mechanism of mine filling material of water-granulated secondary nickel slag. J. Chin. Ceram. Soc. **41**(5), 612–619 (2013)
26. Zhu, L.P., Ni, W., Zhang, X.F., Huang, X.Y.: Performance and microstructure of cemented whole-tailings backfilling materials based on red mud, slag and cement. J. Univ. Sci. Technol. Beijing **32**(7), 838–842 (2013)
27. Chen, G., Liu, Y.P., Fang, Z.Q.: Preparation of calcium carbonate composite filler coated with titanium dioxide and its application in papermaking. J South China Univ Technol. **39**(8), 87–89 (2011)
28. Zhang, H.W., Yu, D.D.: Analysis of pressure-resistance calculating model of carbonnanotubes/carbon black/silicone rubber composite material. J. Funct. Mater. **5**(44), 665–668 (2013)
29. GB 175-2007: *Common Portland Cement*. Standard Press of China, Beijing (2007)
30. GB/T1346-2011: *Test Methods for Water Requirement of Normal Consistency, Setting Time and Soundness of the Portland Cement*. Standard Press of China, Beijing (2011)
31. Ma, X.W., Wang, P.M.: Effects of $P_2O_5$ on the calcination process and hydration of clinker with high content of $C_3S$. J. Mater. Sci. Eng. **28**(1), 26–30 (2010)
32. Lin, K.L., Lin, D.F., Luo, H.L.: Influence of phosphate of the waste sludge on the hydration characteristics of eco-cement. J. Hazard. Mater. **168**(2), 1105–1110 (2009)
33. Khale, D., Chaudhary, R.: Mechanism of geopolymerization and factors influencing its development: a review. J. Mater. Sci. **42**(3), 729–746 (2007)
34. Tong, J., Wang, S., Ma, X.M.: Crystallinity regulation of calcium silicate hydrate and its influence on moisture absorption/desorption properties. Bull. Chin. Ceram. Soc. **38**(1), 83–86 (2019)
35. Lu, Q.M., Zhang, Y.X., Zhang, R.L., Sun, W.B.: Analysis of mechanical properties and microstructure of sludge-ash and cement cementitious system. J Saf. Environ. **19**(1), 308–311 (2019)

36. Xue, P., Xu, A.J., He, D.F., Yang, Q.X., Liu, J.Q., Engström, F., Björkman, B.: Research on the sintering process and characteristics of belite sulphoaluminate cement produced by BOF slag. Constr. Build. Mater. **122**, 567–576 (2016)
37. Zhang, W.S., Zhang, J.T., Ye, J.Y., Qian, J.S., Shen, W.G., Wang, Z.Y.: Structure and activity of dicalcium silicate. J. Chin. Ceram. Soc. **47**(11), 1663–1669 (2019)
38. Xu, Y., Li, J.X., Kan, L.L.: Study on composite cementitious material prepared by calcinating phosphogypsum. Bull. Chin. Ceram. Soc. **33**(4), 953–958 (2014)
39. Mollah, M.Y.A., Kesmez, M., Cocke, D.L.: An X-ray diffraction (XRD) and Fourier transform infrared spectroscopic (FTIR) investigation of the long-term effect on the solidification/stabilization (S/S) of arsenic(V) in Portland cement type-V. Sci. Total Environ. **224**(1), 57–68 (1998)
40. Trezza, M.A., Lavat, A.E.: Analysis of the system $3CaO–Al_2O_3$-$CaSO_4–2H_2O–CaCO_3–H_2O$ by FT-IR spectroscopy. Cem. Concr. Res. **31**(6), 869–872 (2001)
41. Richard, T., Mercury, L., Poulet, F., d'Hendecourt, L.: Diffuse reflectance infrared fourier transform spectroscopy as a tool to characterise water in adsorption/confinement situations. J. Colloid Interface Sci. **304**(1), 125–136 (2006)
42. El-Alfi, E.A., Gado, R.A.: Preparation of calcium sulfoaluminate-belite cement from marble sludge waste. Constr. Build. Mater. **113**(15), 764–772 (2016)
43. Anagnostopoulos, C.A., Sapidis, G., Papastergiadis, E.: Fundamental properties of epoxy resin-modified cement grouts. Constr. Build. Mater. **125**, 184–195 (2016)
44. Kupwade, P.K., Palkovic, D., Bumajdad, A., Sorianoc, C., Büyüköztürk, O.: Use of silica fume and natural volcanic ash as a replacement to Portland cement: Micro and pore structural investigation using NMR, XRD, FTIR and X-ray microtomography. Constr. Build. Mater. **158**, 574–590 (2018)
45. El-Hassan, H., Shao, Y.X.: Early carbonation curing of concrete masonry units with portland limestone cement. Cement Concr. Compos. **62**, 168–177 (2015)
46. Wang, C., Yang, C.H., Qian, J.S., Zhong, M.Q., Zhao, S.: Behavior and mechanism of pozzolanic reaction heat of fly ash and ground granulated blastfurnace slag at early age. J. Chin. Ceram. Soc. **40**(7), 1050–1058 (2012)
47. Zhang, N., Liu, X.M., Sun, H.H.: Hydration characteristics of intermediate-calcium based cementitious materials from red mud and coal gangue. Chin. J. Mater. Res. **28**(5), 325–332 (2014)
48. Zhang, J.W., Guan, X.M., Li, H.Y., Liu, X.X.: Performance and hydration study of ultra-fine sulfoaluminate cement-based double liquid grouting material. Constr. Build. Mater. **132**, 262–270 (2014)